Technical note

In-plane flexure-based clamp

Shorya Awtar*, Jason Meyer Quint

Precision Systems Design Lab, Mechanical Engineering, University of Michigan, 2350 Hayward Street, Ann Arbor, MI 48109, USA

ABSTRACT

This paper presents the design of a simple flexure-based clamp that may be used in experimental set-ups to hold cylindrical and flat components in the plane of a mounting plate. While it is easy to clamp cylindrical components normal to the plane of a mounting plate, effective in-plane clamp designs are relatively less common due to practical fabrication challenges. The proposed design provides a well-distributed clamping force while avoiding localized stress concentration, and is simple to fabricate using standard machining processes. Additionally, it allows adjustability in the axial position of the component being held prior to clamping, and also provides self-aligning and self-correcting capabilities. Several examples where this clamp design has been successfully employed are presented. A simple model is developed to provide physical and analytical insight into the relation between the clamp's geometric dimensions and performance. These results are validated via finite elements analysis. Several alternate in-plane clamp designs are also proposed.

© 2012 Elsevier Inc. All rights reserved.

1. Motivation

In the design of precision experimental set-ups and machines, there is often a need to assemble cylindrical components, for example sensors or actuators, with respect to a mounting plate such that the axis of the component lies in the plane of the plate (Fig. 1). A common example is that of holding a capacitance probe securely to make precise in-plane displacement measurements. The joint or clamp that is employed for this purpose should meet the following general requirements:

1. Foremost, the clamp should provide a secure interface – one that is free of backlash, and creates adequate and distributed clamping force over the length of the component being held to avoid slippage. A loosely held capacitance probe, for example, is prone to inaccurate measurements as well as greater electrical noise. The use of a direct-acting set-screw (Fig. 1a) is non-ideal because it exerts a large localized radial load on the probe, resulting in surface damage and potential loss in calibration. On the other hand, a lightly tightened screw, which might avoid these drawbacks, is prone to coming loose over time and may not provide adequate clamping force. Clamp designs involving two or more counter-acting jaws (Fig. 1b and c) are generally desirable because they overcome all these limitations. However, the

particular designs shown in Fig. 1 are difficult to manufacture, as discussed in point 5 below.
2. The clamp should provide and maintain alignment between the cylinder and the plate. In particular, the location of the component's axis with respect to the plate should be deterministically and accurately established each time this component is mounted on the plate via the clamp. Improper alignment of a capacitance probe with respect to its mounting plate leads to measurement inaccuracies such as cosine errors.
3. Quick and easy clamp engagement and disengagement is important because it might be necessary to assemble and disassemble the component with respect to the plate frequently in an experimental set-up.
4. The ability to adjust the axial location of the component with respect to the plate before clamp engagement is also critical in certain applications. In the case of a capacitance probe, the sensor should be free to move along its axis so it can be optimally located with respect to its target.
5. Manufacturability is one of the most important practical considerations. While the in-plane clamp designs shown in Fig. 1b and c meet the above requirements, these designs are difficult to implement given the challenge in creating 'in-plane cuts', especially if the plate is part of a larger mounting/reference plate. In comparison, it is clearly more feasible and inexpensive to create 'out of-plane' cuts using common processes such as water-jet machining, laser machining, or electric discharge machining (EDM). As a consequence, it is much easier to design and fabricate a clamp, with all the above desired attributes, that holds a

* Corresponding author. Tel.: +1 734 615 0285.
  E-mail address: awtar@umich.edu (S. Awtar).
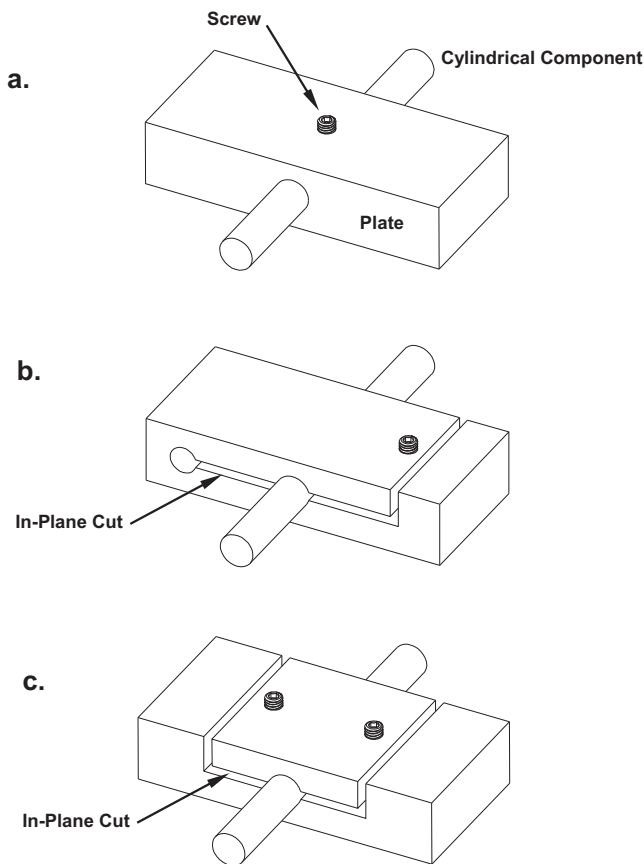
Fig. 1. In-plane clamp examples and challenges.
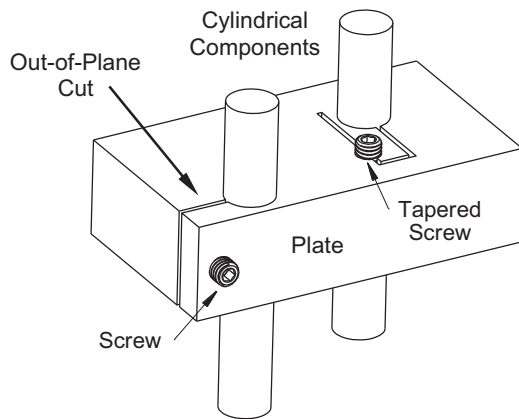
Fig. 2. Out-of-plane clamp examples.

cylindrical component normal to plane of a plate, as shown in Fig. 2.

In this paper, we present the design and validation of a simple flexure-based clamp that meets all of the above requirements for an in-plane assembly. We describe the proposed design and its underlying kinematic principle in Section 2, and cover the practical considerations associated with fabrication and implementation in Section 3. Several examples where this design has been employed are also illustrated. Section 4 provides a simple closed-form analytical model to relate the clamp's geometry to it clamping performance. Key design insights gained through this model are summarized. In Section 5, we validate these closed-form results
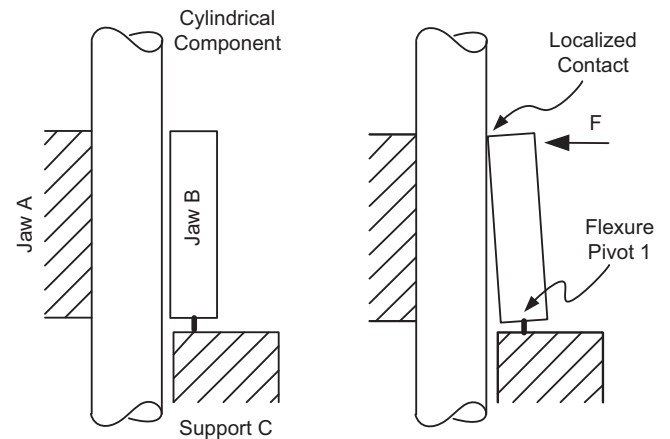
Fig. 3. Sub-optimal in-plane clamp design (non-uniform force distribution).

using finite element analysis. Based on these analytical results, we compile a list of design guidelines in Section 6. Finally in Section 7, we present alternate designs based on the proposed kinematic principle as well as other concepts for clamping cylindrical and flat components in-plane.

2. Proposed flexure-based clamp design

Designs that only require out-of-plane cuts are practical, given the availability of water-jet machining, wire-EDM, laser cutting, etc. An obvious in-plane clamp design that can be created by employing out-of-plane cuts only is shown in Fig. 3. In this clamping arrangement, the cylindrical component is placed between a fixed jaw (A) and a moving jaw (B), which is pivoted about support (C). Jaw (A) and support (C) are part of the same rigid plate. The obvious drawback of this design is that the application of a clamping force (F) on the moving jaw (B) results in a localized contact between the latter and the cylindrical component, as shown. This not only leads to ineffective clamping but can also damage the cylindrical component. The initial gap between the cylinder and jaw (B) is shown exaggerated in this figure to highlight the rotation of the latter upon clamping.

We propose a simple modification to the design in Fig. 4 to overcome this specific problem while meeting the clamping requirements stated in Section 1. Like in the previous case, this clamping arrangement also comprises a fixed jaw (A) and moving jaw (B), with the cylindrical component placed in between. However, the moving jaw (B) is not directly connected to the ground; instead, it is connected via flexure pivot (2) to an intermediate jaw (D), which is in turn connected to the ground support (C) via flexure pivot (1). Both flexure pivots are intended to have a low in-plane rotational stiffness. Pivot (1) ensures that the clamping force (F) applied at jaw (D) is transmitted on to jaw (B). Pivot (2) ensures that while this clamping force is transmitted on to the cylindrical component, jaw (B) remains free to align itself with the cylinder. In other words, pivot (2) prevents the rotation of jaw (D) from being transmitted to jaw (B), and this pivot's low rotational stiffness ensures that only a normal clamping force acts at the middle of jaw (B). This prevents any localized forces and stress concentration as seen in the previous design. Rather, the clamping force distributes itself over the length of jaw (B), as per St. Venant's principle [1], and secures the cylindrical component against the fixed jaw (A). Once again, in Fig. 4, the initial gap between the cylinder and jaw (B) is exaggerated to highlight the rotation of jaw (D).
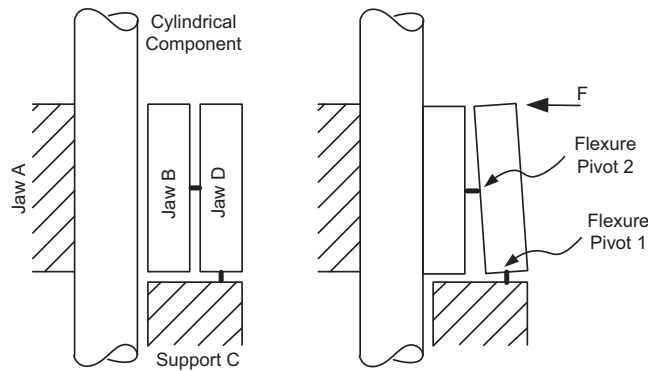
Fig. 4. Proposed in-plane clamp design (uniform force distribution).

This clamp design was first reported in [2], and since then has been employed and validated in several experimental set-ups. The following section discusses how this design can be practically implemented. However, this is not the only flexure-based design that meets the requirements of in-plane clamping. In fact, it is important to recognize the underlying kinematic principle behind the proposed flexure-based clamp design, which is to provide the moving jaw with at least two in-plane degrees of freedom that allow it to line-up with the object being clamped. This is in contrast with the kinematic configuration in Fig. 3, where the moving jaw has a single rotational degree of freedom and therefore cannot freely align itself with the clamped object. Once this kinematic principle is recognized, several other flexure-based clamp design embodiments may be conceived, some of which are illustrated later in Section 7.

The purpose and scope of this paper does not cover a comprehensive comparative study of these various designs. Instead, we use the design of Fig. 4 as an example to present detailed modeling, analysis, and hardware implementation. This choice does not assume or imply that this particular design is superior to the alternate designs in Section 7, or others that may be similarly conceived based on the above kinematic principle.

3. Fabrication and implementation

All features of the clamping arrangement shown in Fig. 4 can be incorporated monolithically in a single plate via a single out-of-plane cut, as shown in an actual implementation of the proposed design in Fig. 5. The in-plane clamping force can be easily applied by means of a National Pipe Thread (NPT) screw, which has a tapered profile. Because of its taper, tightening the screw forces jaw (D) to the left (in Figs. 4 and 5). The overall fabrication of this clamp is also relatively straightforward. First, the entire 2-D pattern can be cut on a flat plate using a process such as water-jet cutting or wire-EDM. Since jaws (B) and (D) in the resulting part are supported merely by the thin flexure pivots (1) and (2), any subsequent machining has to be carefully planned. To machine the in-plane hole that the cylindrical component slides through, these two jaws will have to be temporarily held rigidly in place. This may be accomplished by holding the plate between two sheets of emery paper in a regular vice, such that the emery paper is in contact with the plate and the jaws (B) and (D). As the vice is tightened, the grit particles of the emery paper dig into the faces of the plate, thus immobilizing jaws (B) and (D). Now the plate can be drilled and reamed as though it were a solid block. A spiral flute reamer is recommended because of the discontinuity introduced by the in-plane cut. The reamed hole should be slightly over-sized (<0.001 in. or 0.025 mm) so that it allows the cylindrical component to slide through with ease, while maintaining good axial alignment with the plate. Once the plate
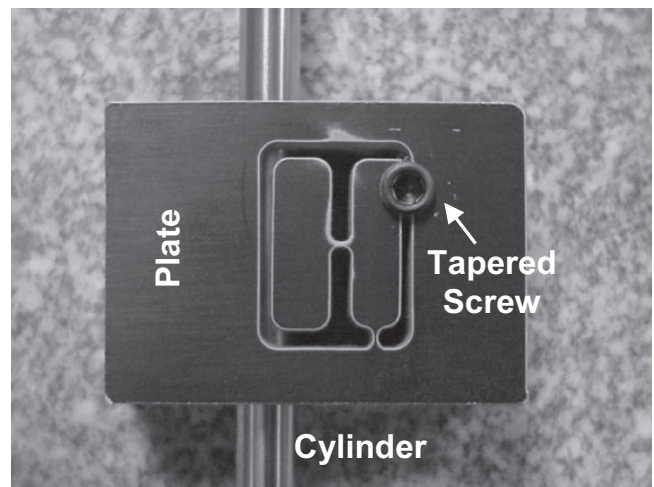
Fig. 5. Proposed in-plane clamp design: physical implementation.

is drilled and reamed, either the cylindrical object or an artifact of the same diameter should be slid into the hole before tapping the NPT threads for the tapered screw. Optionally, this hole may be first counter-bored to a depth such that the subsequent tapered threads lie approximately at half the out-of-plane thickness of the plate. This ensures that the clamping force arising from the tapered screw is generally centered along the out-of-plane depth of jaw (B).

An alternative fabrication approach is to leave supporting tabs or bridges during the initial 2-D cut that keep the jaws (B) and (D) attached to the surrounding plate. These supporting tabs provide adequate rigidity while the in-plane hole is machined. Once this is done, these tabs may be removed by using a fine end mill cutter or a saw blade. If carefully done, these tabs may also be removed via EDM or water-jet. All these additional steps make this second approach slightly more time-consuming. A third approach is to machine the in-plane hole first, and then mount the plate on a water-jet or wire-EDM machine such that the hole is appropriately aligned with the 2-D pattern to be cut. Depending on the machining process used for the 2-D cutting, this alignment will involve additional fixturing and referencing.

We have employed the first fabrication approach described above with repeated success. Fig. 6 illustrates the various experimental set-ups where the proposed flexure clamp has been employed to hold cylindrical components. In Fig. 6a, these clamps are monolithically incorporated into the design of a sensor mount to hold multiple capacitance probes. This sensor mount was used to measure the error motions and cross-axis coupling of a high precision XY flexure stage [2]. As expected, the clamps effectively
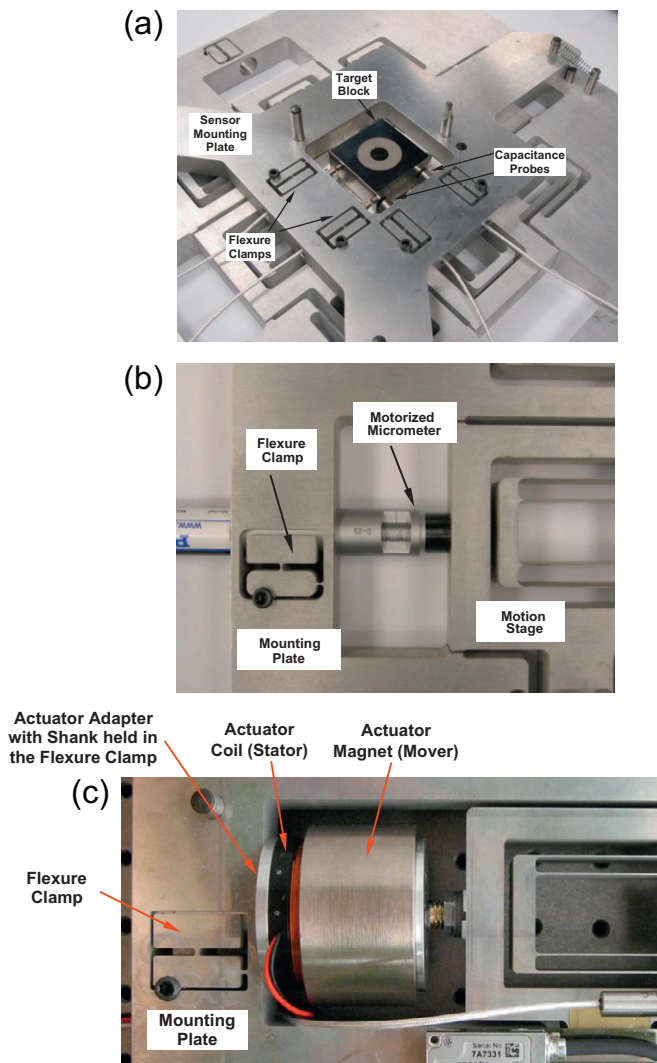
Fig. 6. (a) Capacitance probe mount. (b) Micrometer actuator mount. (c) Voice coil actuator mount.

Fig. 7. (a) In-plane flexure clamp for flat components. (b) Alternate jaw design to minimize micro-slip.

provide a well-distributed force on the probes, while allowing an axial adjustment of the probe position before clamping, and ensuring proper alignment with respect to the mounting plate after clamping.

In Fig. 6b, the proposed clamp design is used to mount a motorized micrometer, intended to apply an in-plane actuation force. It is common for these actuators to include a tightly toleranced cylindrical surface for axial alignment, but no other features that allow mounting on a plate. The proposed clamp proves to be ideal because it securely holds the actuator without damaging its surface or its sensitive internal assembly, while providing the desired alignment of the actuator axis. It also allows considerable ease of set-up and assembly since the actuator can be readily adjusted easily along its own axis prior to clamping. In Fig. 6c, the same clamp design is employed to hold a voice coil actuator via a cylindrical adapter; the above listed benefits hold here as well. In all of these cases, the clamp ensures that the axis of the cylindrical component is repeatability aligned with the axis of the in-plane hole, and therefore the rest of the assembly on the plate. Such alignment and associated repeatability were of utmost importance in these above-mentioned experimental set-ups.

This basic idea of clamping cylindrical objects in planar configurations may be extended to other applications as well. For example,

one may consider holding an optical fiber on a silicon wafer in a MEMS device. In this case also, fabrication of two-dimensional features (out-of-plane cuts) on the wafer is relatively straight-forward.

Although the discussion and examples so far have focused on clamping a cylindrical object in-plane, another useful application of the proposed clamp design has been to hold flat flexure strips in-plane to assemble flexure mechanisms [3,4]. The clamp design for these applications incorporates a uniform gap or slot that the flexure strip or other flat component sits in (Fig. 7a), instead of the in-plane hole when a holding cylindrical object.

Another important consideration in any friction based clamp design is the presence of micro-slip at the interface of the clamped object and the clamp jaws. It has been shown that this micro-slip leads to joint hysteresis, which in turn compromises precision [5]. To mitigate this potential risk, either the fixed jaw (A) or the moving jaw (B) can be designed to incorporate two well-spaced, discrete ribs or tabs as shown in Fig. 7b. This jaw shape along with the proposed clamp geometry ensures that the clamping force is distributed evenly between the two tabs, maintaining high pressure at each location. This reduces the possibility of micro-slip and hysteresis at the joint interface.

As earlier, this clamp design for flat strips can also be incorporated monolithically into the mounting plate using standard fabrication processes. In Fig. 8a, a parallelogram flexure mechanism with three beams was assembled using six flexure clamps – three on a ground frame and three on a moving stage [3]. This single experimental set-up was used to test and characterize flexure beams with a range of shapes, thickness, material choices, and parallelism errors – dozens of variations in all. Making the beams integral with the ground frame and the moving stage would require a separate experimental set-up for each beam variation considered, which would be impractical. Instead, working with the proposed clamps allowed us to create a single experimental set-up
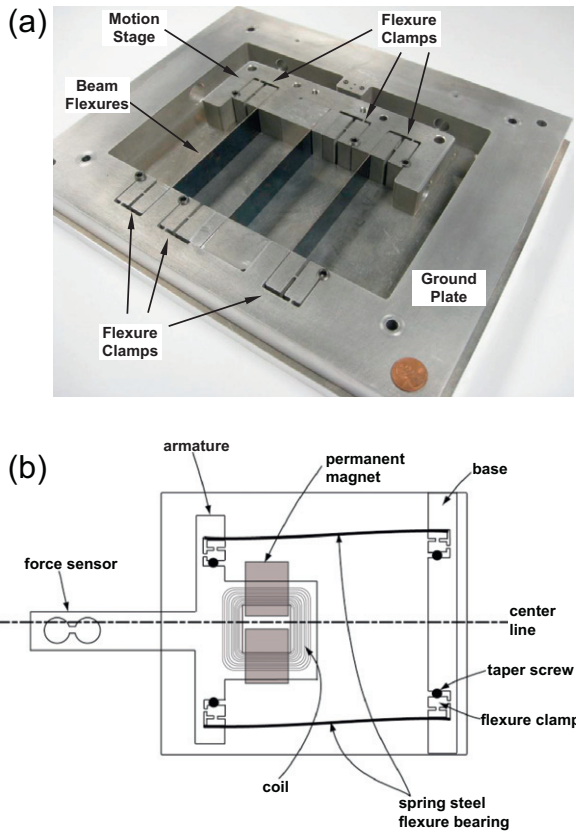
Fig. 8. (a) Reconfigurable 3-beam parallelogram flexure mechanism assembly. (b) Electromagnetic actuator – flexure bearing assembly.

with the appropriate sensing and actuation schemes, while simply replacing the beams from one variation to another. These clamps provided effective clamping action without any slippage, repeatable placement and alignment of the beams, and quick assembly and disassembly. Fig. 8b illustrates another example of an assembled flexure mechanism used as a bearing in an electromagnetic actuator [4]. The clamps in this case allow the assembly of a moving stage made of aluminum (AL6061), which ensures low weight, with blue tempered steel (ASTM A682) shim-stock, which is well-suited for flexure behavior. In general, not just flexure strips, but other flat components may also be clamped or assembled in this fashion.

4. Closed-form modeling of the in-plane flexure clamp

In this section, we present a simple, closed-form quantitative model for the proposed clamp along with qualitative arguments, with the objective of determining how its dimensions affect its clamping performance in terms of the magnitude and distribution of the clamping force. The magnitude of the clamping force ultimately determines how much axial load can be supported between the component being held and the mounting plate, prior to the onset of slippage. The uniformity of the clamping force distribution determines how effective the clamp is.

We consider the case of clamping a flat component rather than a cylindrical component because this allows us to create a simpler, planar or two-dimensional model. However, the conclusions drawn from this planar model are qualitatively valid for all cases. Fig. 9 shows the free body diagrams of the flexure clamp, the fixed jaw, and the component being held. The relevant dimensions of the flexure clamp are also shown. F_o is the in-plane clamp engagement force generated by the tapered screw on jaw (D). $f_c(y)$ represents

the distribution of the clamping force on jaw (B); F_c is the effective sum of this distributed force. F_a is a possible loading force on the component being held, acting along its axis.

The clamp geometry in Fig. 9 is shown in an undeformed configuration. In practice, there is a small initial gap Δ between the component to be held and jaw (B) to allow a slide fit between the mating components before clamping. After clamping, this gap is closed and while jaw (B) remains parallel to the component, jaw (D) rotates to the left by an angle $\theta = \Delta/L_1$. An initial gap $\Delta \sim 0.001$ in. would be typical, and L_1 would be of the order of ~ 1 in. This implies that θ will be of the order of 0.001 rad, which justifies small angle approximations.

The relative rotation of each of the flexure pivots is simply given by θ. L_o and D_2 represent the lengths of pivot (1) and pivot (2), respectively, while K_1 and K_2 represent their torsional stiffness. Creating free body diagrams for jaw (B) and jaw (D), and applying load equilibrium, yields a set of equations that reduce to:

$$F_c = \frac{1}{L_1}\left[F_o L_2 - (K_1 + K_2)\theta - T_{c1}\left(D_1 + \frac{D_2}{2}\right)\right] \quad (1)$$

$$F_c L_5 = K_2\theta - T_{c1}\left(D_3 + \frac{D_2}{2}\right) \quad (2)$$

$$T_{c1} = T_{c2} + F_a \quad (3)$$

The first relation provides an estimate of the magnitude of the clamping force, while the second relation provides an assessment of how symmetrically this force is distributed over the length of jaws (A) and (B). Note that L_5 specifies the location of the effective clamping force F_c but does not necessarily convey the uniformity of the clamping force distribution. Using the first relation, the second relation may be further simplified, as follows:

$$L_5 = L_1 \frac{\left[K_2\theta - T_{c1}(D_3 + (D_2/2))\right]}{\left[F_o L_2 - (K_1 + K_2)\theta - T_{c1}(D_1 + (D_2/2))\right]} \quad (4)$$

For a given clamp engagement force F_o and a clamp loading force F_a, there are four unknowns (F_c, T_{c1}, T_{c2}, and L_5) and only three independent equations, Eqs. (1)–(3). This results in a statically indeterminate condition that cannot be explicitly solved for without taking into consideration contact mechanics. For example, the internal forces T_{c1} and T_{c2} cannot be determined with respect to the clamp dimensions and externally applied forces F_a and F_o; similarly, the actual clamping force distribution $f_c(y)$ is not fully predictable. However, a detailed contact analysis that overcomes these limitations is beyond the scope of this paper. Nevertheless, the simple relations listed above prove to be accurate and provide important design and performance insights, as summarized in the next section.

5. Finite element analysis (FEA) validation and design insights

We created a plane-strain finite element model of the two-dimensional clamp geometry shown in Fig. 9 using ANSYS to validate the above closed-form relations. All components – Ground (C), jaw (A), jaw (B), jaw (D), pivot (1), pivot (2), and the clamped component – were modeled as rectangles and meshed with PLANE82 area-elements. TARGE169 and CONTA172 line-elements were used to capture the frictional contact between the clamped component and Jaws (A) and (B). The clamp jaws, flexure pivots, as well as the clamped component were all assumed to be made from Aluminum 6061 ($E = 68.9$ GPa, $\nu = 0.33$). With reference to Fig. 9, the following nominal dimensions (in millimeters) were used in the FEA: $D_0 = 6$, $D_1 = 6$, $D_2 = 3$, $D_3 = 10$, $D_4 = 2$, $L_0 = 3$, $L_1 = 15.5$, $L_2 = 29.5$, $L_3 = 14$, $L_4 = 14$, and thickness of each flexure pivot $T = 1$. An initial gap, $\Delta = 0.0254$ mm, between jaw (B) and the component to
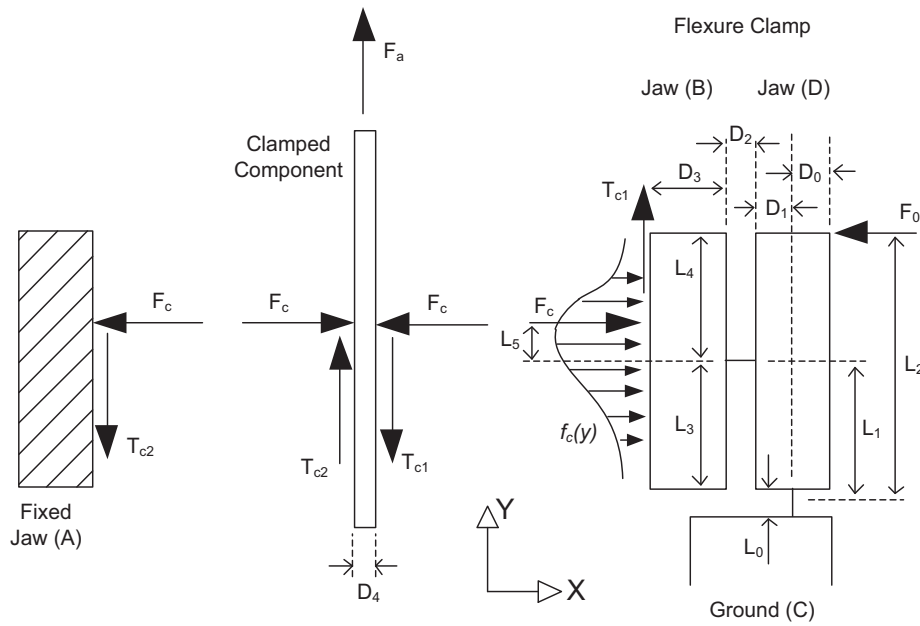
Fig. 9. Flexure clamp dimensions.

be clamped was included in the FEA model. A suitably high mesh resolution (element length of 0.5 mm) was iteratively determined to provide better than 5% convergence on F_c, F_o, and L_5 in the FEA simulations.

It is important to note than in a two-dimensional plane-strain FEA model, the out-of-plane dimension is inconsequential; instead, all force and stress results are reported per unit depth. In the practical examples mentioned in Section 3, we have used plate thickness values ranging from 12.7 to 25.4 mm (or 0.5 to 1.0 in.). FEA validation of the closed-form relations derived in Section 4, along with key observations based on these analytical results are presented next.

I. The equilibrium model represented by Eqs. (1)–(3) agrees with the FEA results. At each step of the FEA, the relevant forces were measured in ANSYS and were found to satisfy these equations within less than 1% error. More specifically, Eq. (1) shows that the engagement force F_o is amplified by the factor L_2/L_1, which serves as a transmission ratio, resulting in a clamping force F_c. It is also clear that the torsional deformation of the flexure pivots tends to reduce the clamping force, and therefore it is desirable to keep θ as well as K_1 and K_2 low. This is inherently ensured by the design – θ indeed is a small number and the flexure pivots offer a low in-plane torsional stiffness because of their geometry. In order to validate the relation given by Eq. (1), a fixed displacement was applied at the upper right corner of jaw (D) in the negative X direction, simulating the effect of tightening a tapered screw. Starting from a value of 52 μm, which is sufficient to close the initial gap of 25.4 μm between jaw (B) and the component, this input displacement was increased in steps of 0.52 μm. At each loading condition, the engagement force, F_o, as well as the total clamping force F_c and traction force T_{c1} were recorded, while keeping F_a zero. A comparison between the closed-form analysis and FEA is plotted in Fig. 10. For any given value of input force F_o, the circles represent values of F_c directly measured using FEA, and the asterisks represent closed-form estimates of F_c. Note that in this and all subsequent figures, the forces are presented as force per unit depth (N/m) of the two-dimensional model. Since Eqs. (1)–(3) are statically inde-terminate, it is not possible to explicitly determine the internal

traction force T_{c1} in closed-form. Therefore, values of T_{c1} mea-sured from FEA and known clamp dimensions are plugged into Eq. (1) to estimate F_c (asterisks in Fig. 10). Because of this non-zero T_{c1}, the scaling factor between F_c and F_o is not simply L_2/L_1 (=1.90), but slightly lower (1.72).

II. For a fixed input displacement, it is not immediately obvious from Eq. (1) how the internal clamping force F_c will respond to the external clamp load F_a, while the input displacement of jaw (D) is held fixed. One may qualitatively observe that a tensile F_a produces an additional CW torque about pivot (1). However, at the same time it also tends to weaken the contact between the component being clamped and jaw (A), thus reducing T_{c2} and associated CW torque about pivot (1). Therefore, it seems that an application of F_a may not influence the clamping force F_c significantly. While this cannot be conclusively determined from the closed-form equations, the FEA results show that this is indeed true. It turns out an increase in F_a is matched by an equal decrease in T_{c2}, and vice versa, thus effectively keeping T_{c1} constant as per Eq. (3). Moreover, FEA also reveals that the
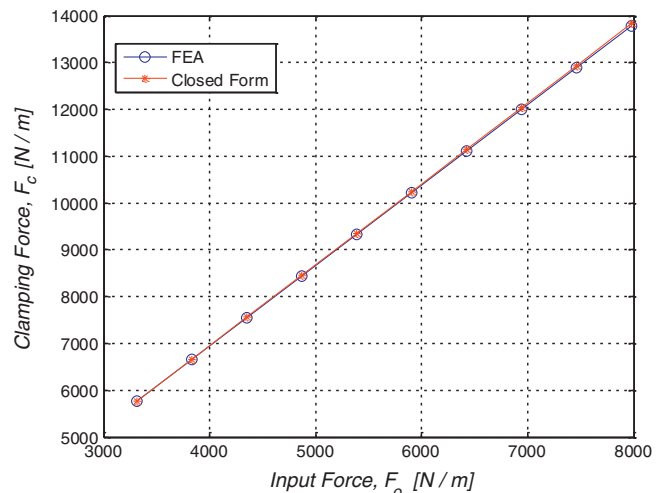
Fig. 10. Clamping force f_c as a function of engagement force F_o.
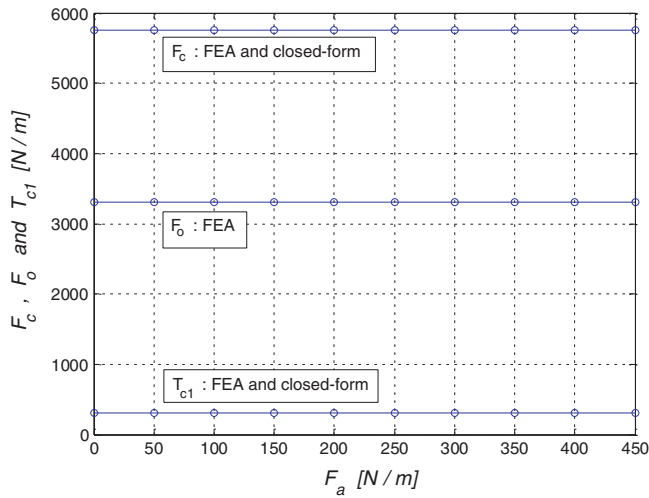
Fig. 11. Variation of clamp internal forces with the axial load.

Fig. 12. Clamp Center of Action location as a function of axial load.

clamp engagement force F_o also remains constant even as F_a varies. With this knowledge, Eq. (1) now clearly indicates that the clamping force F_c is largely insensitive to the axial load F_a. All these observations are reported in Fig. 11, which plots values of the internal forces F_c, F_o, and T_{c1} as F_a is varied while keeping the input displacement at jaw (D) fixed at 52 μm. These internal forces are found to vary by less than 0.1% over the entire range of F_a. Even though these results are presented for a positive F_a, the same conclusions are obtained for a negative F_a as well.

The observation that F_c remains constant as F_a varies highlights the self-correction and performance robustness exhibited by the proposed clamp design. Robustness here implies that the clamping performance is insensitive to variations in the operating conditions such as the loading force F_a. This has obvious positive implications, for example in Fig. 6b, where the flexure clamp is employed to hold a motorized micrometer in place. Upon actuation, the micrometer tip displaces the Motion Stage, thereby exerting as well as experiencing an axial load F_a, which has to be supported by the clamp. However, irrespective of this axial load and its direction, the clamping force F_c and therefore clamping effectiveness remain largely invariant as seen above. In the absence of this self-corrective attribute of the proposed flexure clamp, the presence of F_a could have increased F_c potentially damaging the micrometer housing, or reduced F_c compromising the clamp effectiveness.

III. Eq. (4) provides some insight on how the Center of Action of the distributed clamping force $f_c(y)$, characterized by the dimension L_5, varies. Recognizing that the angle θ and the stiffnesses K_1 and K_2 are small, this equation may be simplified to:

$$L_5 \approx L_1 \frac{\left[-T_{c1}(D_3 + (D_2/2))\right]}{\left[F_o L_2 - T_{c1}(D_1 + (D_2/2))\right]}$$

As discussed in Point II above, for a fixed input displacement of Jaw (D), the clamp internal forces including F_c, F_o, and T_{c1} remain insensitive to the axial load F_a. It has also been shown above that T_{c1} is much smaller compared to F_o. As a result, L_5 is not only small compared to L_1, it also remains invariant with respect to axial load F_a once the clamp has been tightened. This observation is corroborated by FEA in Fig. 12.

Over the range of F_a plotted, the Center of Action moves by less than 0.06 mm, which is insignificant when compared to contact length of jaw (B), $L_3 + L_4 = 28$ mm. While results are reported for positive F_a only, a similar outcome is obtained for negative values
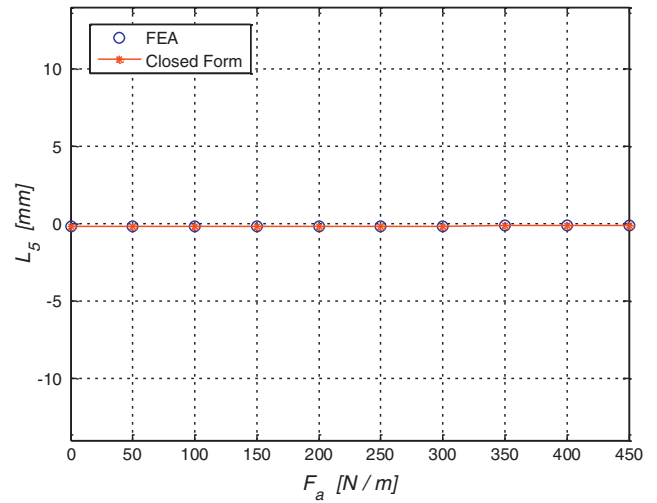
of F_a as well. This observation, once again, reinforces the self-correction and performance robustness of the proposed flexure clamp design. Once the clamp has been tightened using the tapered set-screw, any axial load F_a has very little effect on the clamping force F_c and its Center of Action L_5, thus maintaining the effectiveness of the clamp.

IV. It is important to note that while L_5 captures the symmetry of the clamping force distribution $f_c(y)$ on jaw (B) about pivot (2), it does not reflect on the uniformity of this distribution. The closed-form equilibrium equations, given their static indeterminacy, provide no such insight. However, based on St. Venant's principle, one may qualitatively argue that if D_3 is adequately large, then a point load transmitted from jaw (D) to jaw (B) at pivot (2) will spread out to a more uniform force distribution at the clamped object. This qualitative argument is indeed found to be true via FEA simulations in which the input displacement was fixed at 52 μm, and D_3 was varied. Fig. 13 illustrates the increase in the uniformity of the clamping force distribution as D_3 is increased while all other dimensions are kept the same. On the horizontal axis of this plot, 0 mm corresponds to the top of jaw (B) and 28 mm corresponds to its bottom. The distribution also appears to be largely symmetric, which agrees with the small value of L_5 reported above.

V. Finally, the critical axial load F_a at which the clamped component might slip is important to the designer. From the free body diagrams in Fig. 9, it is clear that the clamped object will slip under a positive axial load when:

$$F_a > T_{c1} - T_{c2} \tag{5}$$

When the external axial load F_a is increased, the internal traction forces T_{c1} and T_{c2} adjust themselves to resist this external load. However, the maximum achievable internal traction forces depend on the coefficient of friction between the flexure clamp jaw material and the object being held, as given by the following relations:

$$T_{c1} \leq \mu F_c \quad \text{and} \quad -T_{c2} \leq \mu F_c \tag{6}$$

Combining Eqs. (5) and (6), and also considering the case when F_a is in the negative direction, the condition for slippage in either direction may be summarized as:

$$|F_a| > 2\mu F_c$$
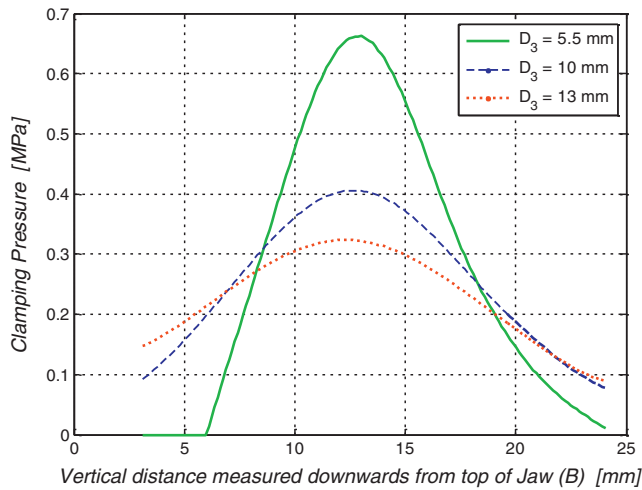
Fig. 13. Clamping pressure distribution on jaw (B).

Substituting F_c from Eq. (1) and ignoring the contribution of angle θ and stiffness K_1 and K_2, this slippage condition may be expressed as:

$$|F_a| > \frac{2\mu}{L_1}\left[F_o L_2 - T_{c1}\left(D_1 + \frac{D_2}{2}\right)\right] \tag{7}$$

For the FEA simulations reported above, F_o and T_{c1} are approximately equal to 3312 N and 310 N, respectively, and a representative coefficient of friction of 0.61 is used. As discussed previously, both these forces remain largely independent of the axial loading F_a. Thus, based on Eq. (7), it may be predicted that slippage would happen in either of the following two cases:

$$F_a < -3440\,\text{N} \quad \text{or} \quad F_a > 4060\,\text{N} \tag{8}$$

Once again, we would like to remind the reader that the force values mentioned here are for an assumed theoretical depth of 1 m, and should be interpreted as being force per meter of depth. These predictions were corroborated by an FEA of the contact and slippage. Holding the input displacement of Jaw (D) fixed at 52 μm, the object slipped for a positive F_a value of 3875 N, which is 5% smaller than the value predicted above. In a separate FEA simulation, where the axial load was applied in the negative direction, the object slipped for an F_a value of −3300 N, which is 4% smaller in magnitude than the above prediction of −3440 N. Thus, the slippage conditions based on the closed-form relations are adequately validated by the FEA results.

We conclude this section with the observation that while a planar clamp design was considered here for the sake of modeling simplicity, the design of Fig. 5 that clamps a cylindrical object can also be investigated using FEA to yield similar outcomes.

6. In-plane flexure clamp design guidelines

Next, the closed-form model and FEA results presented in the previous section may be used to provide some general design guidelines to achieve improved clamping performance.

a. The ratio L_2/L_1 can be increased, within the constraints of the geometric layout, to achieve a larger clamping force F_c for a given engagement force F_o.
b. The rotational stiffness values K_1 and K_2 should be minimized to achieve the largest possible clamping force F_c for a given engagement force F_o. This dictates the flexure pivot dimensions T, D_2 and L_0. Standard guidelines for designing flexural pivots may be considered [6–8]. In an attempt to minimize K_1 and K_2, the user should be careful not to make the pivots too long

and thin, especially Pivot (2), which may be prone to localized buckling. On the other extreme, short and stubby flexure pivots not only negate the clamping force, but are also prone to plastic yielding due to higher stresses. In the application examples cited in Section 3, we have used flexures with dimensions $T = 1\,\text{mm}$ and $D_2 = L_0 = 3\,\text{mm}$ on a 25.4 mm thick AL6061 plate, all of which could be reliably achieved with water-jet cutting and wire-EDM. The resulting rotational stiffness K_1 and K_2 were 48.7 N-m.
c. The overall jaw (B) engagement length, $L_3 + L_4$, should be 2–3 times the diameter of the cylindrical object being clamped, or approximately equal to the depth of the planar object being clamped [9]. Since L_5 has been shown to be small previously, L_3 should be set equal to L_4 to ensure a symmetric clamping force distribution about pivot (2).
d. D_3 should be set to at least 50% of $L_3 + L_4$, and if possible more, in order to achieve uniformity in the clamping pressure distribution as per St. Venant's principle.
e. A similar observation may be made about the dimension D_0, which does not appear in any of the relations presented so far. Since the clamp engagement force F_o is applied at a certain location along the Z axis (normal to the plane of Fig. 9) where the tapered set-screw is located, the dimension D_0 plays an important role in ensuring that the input force is uniformly distributed over the entire depth of the jaw (B) at the location of pivot (2). By St. Venant's principle, $(D_0 + D_1)$ should be of the order of the out-of-plane thickness of the mounting plate. Note that dimensions D_2 and D_3 also help make the clamping force $f_c(y)$ more uniform along the depth of the mounting plate.
f. The size of the tapered set-screw or pipe-plug may be selected based on the size of the flexure clamp and space constraints. Thread pitch determines the sensitivity of the clamp, i.e. number of set-screw turns required to engage or disengage the clamp, and may be selected based on the user's preference.

The above points are based on the previously presented closed-form and finite element analyses. These points serve as qualitative design guidelines that should be considered in the context of other design constraints, such as overall size, available space, assembly, packaging, etc. In practice, the proposed in-plane flexure clamp design has been found to be inherently robust and has worked quite effectively in several of our experiments without much geometric optimization. Our objective in this paper has been to share this simple yet useful design with the precision engineering community. The key attributes of the proposed in-plane flexure clamp are, once again, summarized below:

i. The clamp provides a uniformly distributed clamping force without any local stress concentration that might damage the component being clamped.
ii. It employs a simple flexure-based design that is easy to fabricate and implement. The clamp can be monolithically integrated within the mounting plate, without any additional parts or assembly. Clamp engagement and disengagement merely requires turning a set-screw.
iii. The clamp offers self-alignment functionality to properly position the clamped object with respect to the mounting plate.
iv. Prior to clamp engagement, the design allows easy adjustment of the object being held along its own axis.
v. The clamp exhibits a self-correction capability such that the clamping force and Center of Action remain insensitive to axial loads applied on the object that is held.
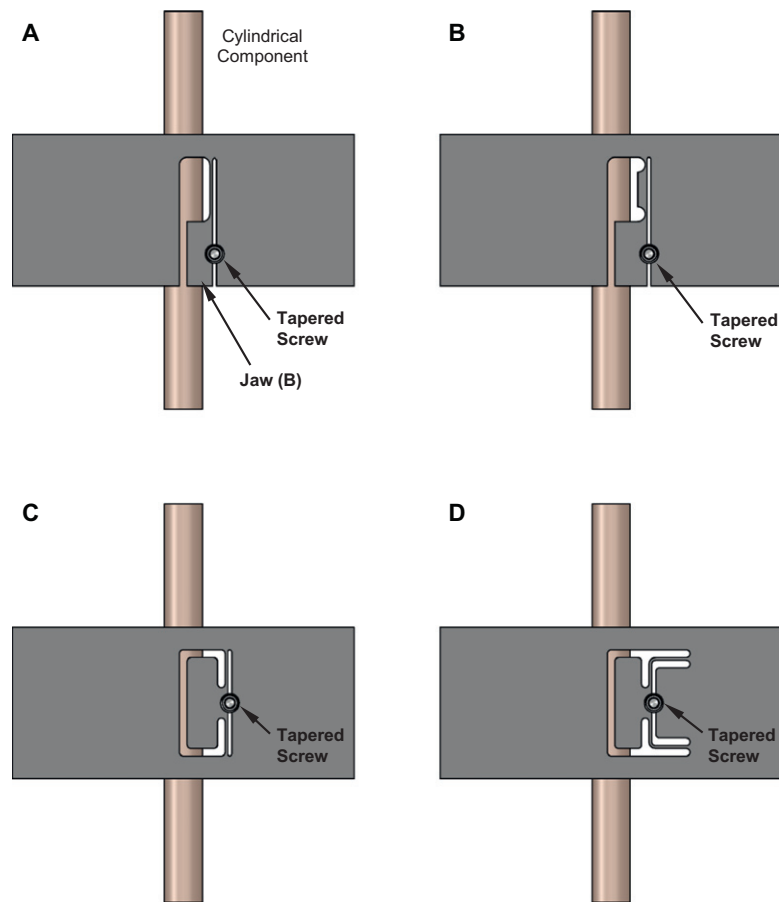
Fig. 14. Alternative in-plane flexure-based clamp designs.

7. Alternate in-plane flexure-based clamp designs and concepts

Next, we present some additional designs for clamping components in-plane in experimental set-ups. The first set of these alternate designs, illustrated in Fig. 14 for the case of clamping cylindrical components, are based on the same kinematic principle as the original design of Fig. 4. In each case, the moving jaw is provided with two in-plane degrees of freedom to allow it to line up with the cylindrical component being held.

The design of Fig. 14a merges the functionality of jaw (D) and flexure pivots (1) and (2) of the original design into a single flexure beam, and the set-screw acts directly on jaw (B). Fig. 14b offers a minor variation of the same design, but with lumped compliance flexure pivots instead of distributed compliance flexure beams. Given the orientation of the flexure beam and pivots in these two designs, it would be easier to insert the component into the plate from the top. Inserting it from the bottom might cause the component to catch due to friction from jaw (B). This potential drawback maybe neutralized via the symmetric design of Fig. 14c. However, if the initial gap between the component and jaw (B) is too large before clamping, the thin flexure beams may experience a build-up of axial stress upon clamping and could potentially yield. This axial stress build-up and risk of yielding may be mitigated via the slightly modified flexure beam geometry of Fig. 14d. These designs have not been analyzed in detail, but are presented here for the benefit of the reader. In terms of ease of manufacturing, these designs are comparable to the original design of Fig. 4. Each option requires the same fabrication set-up with a single 2-D cut. While the

elimination of jaw (D) in the designs of Fig. 14 make them more compact, its inclusion in the design of Fig. 4 helps provide clamping force amplification via the L_2/L_1 ratio, as explained in Section 6. The presence of jaw (D) also increases the distance between the engagement force F_0 and the interface between jaw (B) and the clamped object. As shown earlier, this provides a more uniform clamping force distribution due to St. Venant's principle. To achieve comparable uniformity, jaw (B) in the designs of Fig. 14 would have to be made adequately wide.

From a qualitative stand-point, the differences between these various designs are minor and it is not possible to definitively say if any one is superior compared to the others without a detailed analysis of each. Such an exhaustive, analytical comparison is beyond the scope of this paper. However, an interested designer could perform an analysis analogous to that presented in Sections 4 and 5 for any of the other designs in Fig. 14.

Other than flexure-based clamps, there are other concepts as well that could be considered for holding cylindrical objects in-plane, especially when the mounting plate thickness is adequate. One example is shown in Fig. 15a, where a split bushing or sleeve is used between the mounting plate and the component. Here, a regular set-screw acts on the split bushing instead of acting directly on the component, as was the case in Fig. 1a. The set-screw causes the bushing to close and clamp the component, without locally damaging the latter. Ideally, the sleeve wall should be thin enough so that the sleeve can elastically close in response to the applied force and yet thick enough so that the localized set-screw force at its outer diameter gets distributed along its length at its inside diameter. Choosing a relatively softer material
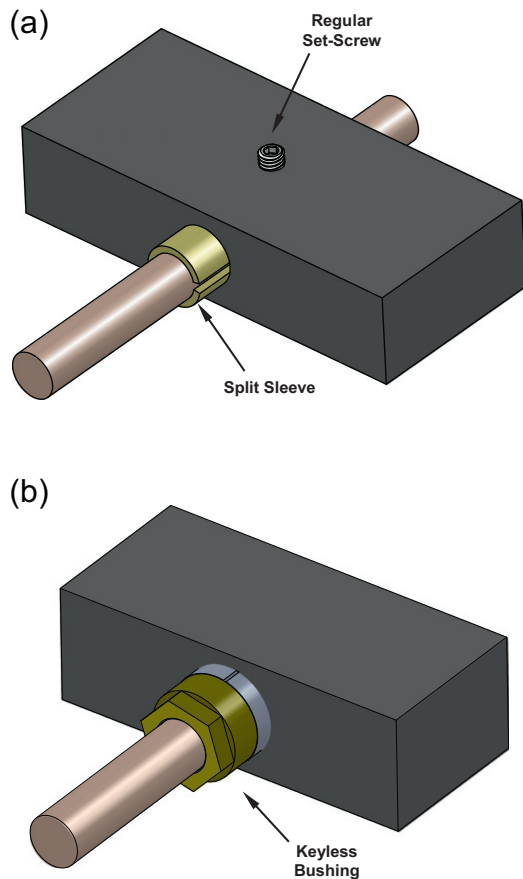
Fig. 15. (a) In-plane clamping using a split bushing/sleeve. (b) In-plane clamping using a keyless bushing.

such as brass or bronze for the sleeve, especially if the component is made of steel, helps distribute the clamping force more effectively.

Yet another effective in-plane clamping option is shown in Fig. 15b that utilizes a keyless bushing from Fenner Drives [10]. The keyless bushing itself comprises three arc-shaped jaws that radially converge to clamp the cylindrical component as the nut is tightened. This principle of operation is analogous to that of a collet used to hold a cylindrical part on a lathe. The obvious limitation of this concept is that it requires a much thicker mounting plate to accommodate a given cylindrical component. For example, for an object with a diameter of 0.5 in., one would require a keyless bushing with an outside diameter of 0.875 in., which in turn would require a plate that is at least 1.125 in. thick. On the other hand, the in-plane flexure clamp design proposed in this paper would only require a 0.75 in. thick plate.

References

[1] Love AEH. A treatise on the mathematical theory of elasticity. Cambridge University Press; 1927.
[2] Awtar, S. Analysis and synthesis of planer kinematic XY mechanisms, Sc.D. Thesis, Massachusetts Institute of Technology, Cambridge, MA, 2004.
[3] Awtar S, Shimotsu K, Sen S. Elastic averaging in flexure mechanisms: a three-beam parallelogram flexure case study'. ASME Journal of Mechanisms and Robotics 2010;2(4).
[4] Gillespie RB, Yu B, Grijalva R, Awtar S. Characterizing the feel of the piano action, Computer Music Journal, MIT Press, 2011;35(1).
[5] Soemers HMJR. Design principles for precision mechanisms, T-Point print VoF, ISBN 978-90-365-3103-0, Chapter 4, 2010.
[6] Xu W, King T. Flexure hinges for piezoactuator displacement amplifiers: flexibility, accuracy and stress consideration. Precision Engineering 1996;19(1).
[7] Lobontiu N, Paine JSN, Garcia E, Goldfarb M. Corner-filleted flexure hinges. ASME Journal of Mechanical Design 2001;123(3).
[8] Wu YF, Zhou ZY. Design calculations for flexure hinges. Review of Scientific Instruments 2002;73(8).
[9] Slocum AH. Precision machine design. Dearborn, MI: Society of Manufacturing Engineers; 1992.
[10] Keyless Bushings & Specialty Locking Devices Catalog, Fenner Drives, Manheim, PA, URL: http://www.fennerdrives.com/catalogs/keyless_bushings.pdf [accessed 30.10.11].